land

MDPI

Article

An Upscaling-Based Strategy to Improve the Ephemeral Gully Mapping Accuracy

Solmaz Fathololoumi [1], Daniel D. Saurette [1], Harnoordeep Singh Mann [1], Naoya Kadota [1], Hiteshkumar B. Vasava [1], Mojtaba Naeimi [1], Prasad Daggupati [2] and Asim Biswas [1,*]

[1] School of Environmental Sciences, University of Guelph, Guelph, ON N1G 2W1, Canada; sfatholo@uoguelph.ca (S.F.); dsaurett@uoguelph.ca (D.D.S.); harnoord@uoguelph.ca (H.S.M.); nkadota@uoguelph.ca (N.K.); hvasava@uoguelph.ca (H.B.V.); mnaeimi@uoguelph.ca (M.N.)
[2] School of Engineering, University of Guelph, Guelph, ON N1G 2W1, Canada; pdaggupa@uoguelph.ca
* Correspondence: biswas@uoguelph.ca; Tel.: +1-519-731-6252

Abstract

Understanding and mapping ephemeral gullies (EGs) are vital for enhancing agricultural productivity and achieving food security. This study proposes an upscaling-based strategy to refine the predictive mapping of EGs, utilizing high-resolution Pléiades Neo (0.6 m) and medium-resolution Sentinel-2 (10 m) satellite imagery, alongside ground-truth EGs mapping in Niagara Region, Canada. The research involved generating spectral feature maps using Blue, Green, Red, and Near-infrared spectral bands, complemented by indices indicative of surface wetness, vegetation, color, and soil texture. Employing the Random Forest (RF) algorithm, this study executed three distinct strategies for EGs identification. The first strategy involved direct calibration using Sentinel-2 spectral features for 10 m resolution mapping. The second strategy utilized high-resolution Pléiades Neo data for model calibration, enabling EGs mapping at resolutions of 0.6, 2, 4, 6, and 8 m. The third, or upscaling strategy, applied the high-resolution calibrated model to medium-resolution Sentinel-2 imagery, producing 10 m resolution EGs maps. The accuracy of these maps was evaluated against actual data and compared across strategies. The findings highlight the Variable Importance Measure (VIM) of different spectral features in EGs identification, with normalized near-infrared (Norm NIR) and normalized red reflectance (Norm Red) exhibiting the highest and lowest VIM, respectively. Vegetation-related indices demonstrated a higher VIM compared to surface wetness indices. The overall classification error of the upscaling strategy at spatial resolutions of 0.6, 2, 4, 6, 8, and 10 m (Upscaled), as well as that of the direct Sentinel-2 model, were 7.9%, 8.2%, 9.1%, 10.3%, 11.2%, 12.5%, and 14.5%, respectively. The errors for EGs maps at various resolutions revealed an increase in identification error with higher spatial resolution. However, the upscaling strategy significantly improved the accuracy of EGs identification in medium spatial resolution scenarios. This study not only advances the methodology for EGs mapping but also contributes to the broader field of precision agriculture and environmental management. By providing a scalable and accessible approach to EGs mapping, this research supports enhanced soil conservation practices and sustainable land management, addressing key challenges in agricultural sustainability and environmental stewardship.

Keywords: ephemeral gullies; soil erosion; satellite imagery; upscaling strategy; precision agriculture; environmental management

check for updates

Academic Editor: Arjun Heimsath

Received: 10 May 2025
Revised: 5 June 2025
Accepted: 20 June 2025
Published: 24 June 2025

Citation: Fathololoumi, S.; Saurette, D.D.; Mann, H.S.; Kadota, N.; Vasava, H.B.; Naeimi, M.; Daggupati, P.; Biswas, A. An Upscaling-Based Strategy to Improve the Ephemeral Gully Mapping Accuracy. *Land* **2025**, *14*, 1344. https://doi.org/10.3390/land14071344

Copyright: © 2025 by the authors. Licensee MDPI, Basel, Switzerland. This article is an open access article distributed under the terms and conditions of the Creative Commons Attribution (CC BY) license (https://creativecommons.org/licenses/by/4.0/).

1. Introduction

Gully erosion is known as one of the most important environmental hazards in the world, which has many negative effects and consequences in the fields of agriculture, natural resources, hydrology, etc., [1]. These gullies can be divided into permanent and ephemeral groups, where ephemeral gullies (EGs) are small rills and channels that occur due to the concentration of surface runoff flow in a channel or the penetration of subsurface flow into underground paths and the collapse of these paths [2]. These gullies can contribute more than 40% of the sediments delivered to the edges of agricultural fields and thus endanger the health and ecological services of the downstream areas [3]. The highest frequency of spatial distribution of EGs is in agricultural fields, therefore, they directly affect the performance of agricultural production and, as a result, food security [4,5]. Therefore, identifying the location of EGs and calculating the amount of erosion associated with them is crucial for designing and implementing agricultural land protection programs [6].

It is important to distinguish ephemeral gullies from rills, as both are forms of concentrated flow erosion but differ in scale, formation, and management implications. Rills are small, shallow channels typically less than 30 cm deep, which are often eliminated by routine tillage. In contrast, ephemeral gullies are larger features often deeper and wider that recur in the same locations and require more intensive mechanical interventions for removal. Unlike rills, EGs are more persistent and can cause significant off-site sediment transport. Their identification through remote sensing is more feasible due to their size, although the spectral similarity with rills presents challenges. Unlike permanent gullies, EGs are short-lived and often small in size, forming quickly during heavy rainfall events and disappearing due to tillage or vegetation growth. Their narrow width, shallow depth, and temporal variability make them particularly challenging to detect using conventional field surveys or satellite imagery, especially in large agricultural areas. These characteristics demand high-resolution data and advanced analytical techniques for accurate mapping [7]. In the past years, many efforts have been made to develop models for identifying EGs [8,9]. Although they all have similar goals, the approaches differ in terms of data collection methods, effective features, and model selection. In the first approaches, the data collection is divided into field-based and remote sensing (RS)-based methods. Field-based methods are simple and require little data; however, identifying EGs based on these approaches in large areas is costly and time consuming [10–12]. RS-based techniques are widely used to identify EGs and their spatial and temporal changes in large areas. The focus of recent studies has been on the use of these latter approaches in identifying EGs [6,13]. Casalí et al. [14] evaluated the accuracy of three field methods for measuring rill and ephemeral gully erosion. They found that method choice and channel shape strongly influence measurement errors. The micro-topographic profile meter was the most reliable, while simplified or poorly matched methods led to significant inaccuracies even with frequent sampling.

In terms of the type of effective features, the approaches used to identify EGs based on RS can be divided into topographic features-based and spectral and biophysical features-based approaches. Given the nature and occurrence of gullies in the landscape, the first features used to identify them were topographical features [15,16]. It was also shown in a number of studies that considering spectral and biophysical features, in addition to topographical features, can increase the accuracy of identifying EGs [17,18]. In many regions of the world, it is challenging to access topographic data with appropriate spatial (1–2 m approximately) and temporal (daily–monthly approximately) resolution to identify EGs and their spatiotemporal changes. However, due to an abundance of satellite image data with different spatial, temporal, and spectral resolutions around the globe, access to spectral and biophysical features is easier than topographical features. Therefore, the

development of models based on spectral and biophysical features in identifying the quantity and quality of EGs can be very useful in terms of cost, time, and implementation.

The approaches to identify EGs can be divided into (1) classification-based approaches, (2) regression-based models, (3) spatial multi-criteria analysis models, and (4) machine learning and artificial intelligence-based models. Each of these models has its own advantages and disadvantages that have been discussed in various studies [17,19–21]. Among the various modeling approaches used for EG identification, machine learning algorithms, particularly Random Forest (RF), have gained prominence due to their superior performance in handling high-dimensional and non-linear data. Unlike traditional regression models or spatial multi-criteria analysis, RF does not assume linearity or normality and can model complex relationships between spectral indices and EG presence. It is also less sensitive to noise and overfitting, thanks to its ensemble structure based on decision trees and bootstrap aggregation. Additionally, RF provides valuable insights into feature importance, which is critical for identifying the most effective spectral indicators in EG detection. These advantages make RF especially suitable for remote sensing applications where input data can be heterogeneous and noisy. These advantages make RF a practical and interpretable choice over other classifiers such as SVM, logistic regression, or ANN.

The identification of EGs is more complicated than for other types of gullies due to their small size, spatial heterogeneity, pattern, shape, and rapid variability [22,23]. Therefore, to identify these gullies, effective features with high spatial resolution are needed. These effective features can be prepared from a digital elevation model (DEM) and satellite images with high spatial resolution or data obtained from short-range photogrammetry such as drones. In previous studies, it was shown that the developed approaches based on these data were effective for identifying EGs in small areas [6,24]. However, working based on these data to identify EGs for large areas is not only very time-consuming and expensive, but also requires very advanced processing systems for large-scale data analysis. One of the important factors for evaluating the efficiency of the developed approaches is their generalizability for different spatial resolutions. Nowadays, the development and evaluation of suitable models for identifying EGs based on features that can be extracted from satellite images with medium spatial resolution that are free and provide global coverage can be very necessary and useful for managing and reducing the effects of this phenomenon.

Recent advances in machine learning have significantly improved the ability to detect ephemeral gullies from remote sensing data. Studies employing deep learning, support vector machines, and ensemble methods like Random Forest have shown promise in capturing the subtle spatial patterns of EGs, particularly in high-resolution imagery (e.g., [22,24]). Fathololoumi et al. [25], using multi-classifier ensemble models and high-resolution Pléiades-1 imagery, have shown that integrating multiple classifiers can enhance EG mapping accuracy at a local scale. However, most of these approaches are limited to small-scale applications due to computational demands and the high cost of detailed imagery. In this context, the present study introduces an upscaling-based strategy that leverages high-resolution model training to improve EG detection in medium-resolution satellite data, offering a scalable and practical alternative for large-area mapping. High-resolution imagery has been shown to substantially improve the accuracy of EG mapping due to its ability to capture fine-scale surface features. However, its high acquisition cost and intensive computational requirements pose significant limitations for large-scale or repeated monitoring efforts. These challenges underscore the need for innovative, scalable approaches, such as upscaling that can extend the benefits of high-resolution model calibration to widely available medium-resolution satellite data. Addressing this gap, the

present study proposes an upscaling-based strategy designed to enhance the accuracy and scalability of EG detection across broader agricultural landscapes.

In this study, the possibility of identifying EGs based on spectral and biophysical features that can be extracted from satellite images with different spatial resolution is evaluated. The main objective of this study was to propose an upscaling-based strategy to improve the accuracy of EGs mapping. In the first strategy, the EGs identification model was directly calibrated based on the spectral features extracted from the medium spatial resolution image and was used to prepare EG maps with a 10 m spatial resolution (direct strategy). In the second strategy, the EGs identification model was calibrated based on spectral features extracted from high spatial resolution imagery and for the creation of EGs maps with a spatial resolution of 0.6, 2, 4, 6, and 8 m based on the spectral features of upscaled images. In the third strategy, the calibrated model based on the second strategy was implemented on spectral features extracted from medium spatial resolution and the EGs map was created with spatial resolution of 10 m (upscaling strategy). Finally, the efficiency of three scenarios in extracting EGs is compared. Also, the sensitivity of identifying EGs was evaluated with respect to spatial resolution based on satellite data.

2. Study Area

A field with several EGs located in the Niagara Region of southern Ontario, Canada was selected as a test site for this study. In this field, EGs are filled by plowing and tillage operations, but become visible with the onset of rain and reach their most severe state in winter when the crop is harvested and left without cultivation (Figure 1a). The selected field is located at (43.13° latitude and −79.29° longitude) (Figure 1b). The area of the field site under study is 0.97 km^2 and the area where EGs occur occupies approximately 0.0786 km^2. Field observations indicated the co-occurrence of both ephemeral gullies and rills within the study site. However, ephemeral gullies were observed to form in specific, recurring locations, often aligned with concentrated surface runoff pathways. These features were typically deeper and more distinct than rills and remained visible throughout the wet season. While rills were more numerous and occurred across wider areas, they were shallow and generally removed during post-harvest tillage. Therefore, the EGs were the primary focus of this study due to their larger geomorphic impact and suitability for detection in satellite imagery.

Southern Ontario, particularly the Niagara Region, is among Canada's most agriculturally intensive areas, producing a substantial share of the nation's food supply [26,27]. This region is characterized by row cropping systems—mainly corn and soybeans—commonly managed through conventional tillage, which leaves soil surfaces exposed and vulnerable to erosion. The soil, primarily silty clay loam, is moderately to highly susceptible to detachment under rainfall-driven runoff. Combined with gently to moderately sloped terrain (average gradient ~5%) and slope lengths ranging from 50 to 150 m, these conditions create a high potential for ephemeral gully formation. Seasonal rainfall, especially during spring and fall storms, further exacerbates surface runoff, while reduced vegetation cover after harvest contributes to concentrated flow paths along field boundaries and machinery tracks. These environmental and land management factors make the Niagara Region a representative and relevant site for studying ephemeral gully development in intensively farmed landscapes.

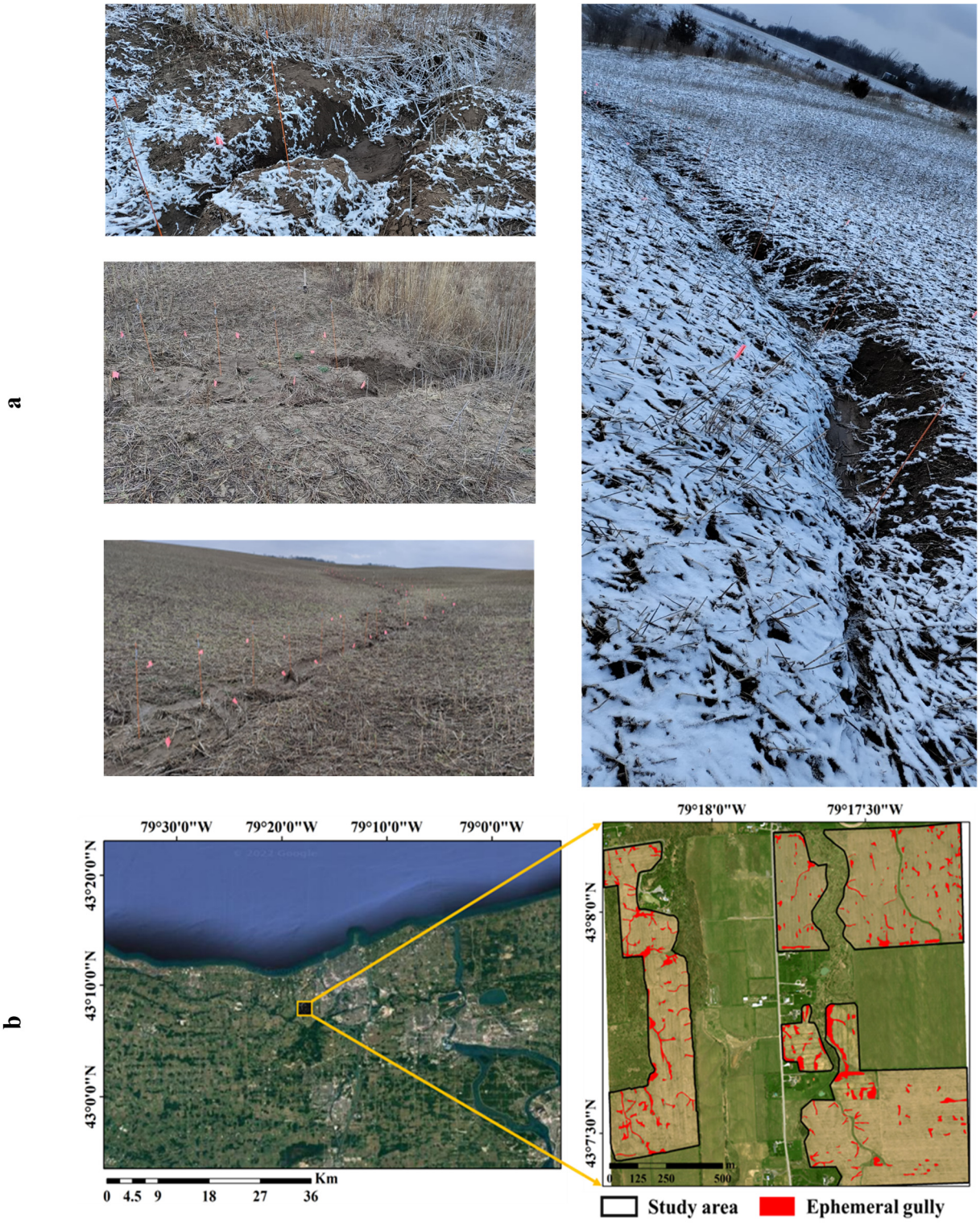

Figure 1. Photos of ephemeral gullies (EGs) during winter in the study area (**a**) and geographical location of study area and mapped EGs in study area (**b**).

3. Data and Methods

3.1. Data Collection and Preparation

The selection of the study region in Southern Ontario, specifically the Niagara Region, was informed by the prevalence of ephemeral gullies (EGs), as identified during field visits. A detailed EGs map for the area was generated through manual digitization and visual

interpretation of high-resolution satellite imagery. For manual digitization, the Editor tool in Arc map 10.3 software was used.

For model training and calibration, a dataset comprising 367 pixels representing EGs and 346 pixels for non-EGs was randomly selected from the actual EGs map. The remaining areas served as validation zones. The total EGs coverage in the study area was quantified at 0.0786 km^2.

The study utilized both medium and high spatial resolution satellite imagery, integrated with field-collected EGs data, to construct a robust training dataset. This dataset was pivotal in calibrating and validating various EGs identification models. The satellite data comprised Sentinel-2 and Pléiades Neo imagery, representing medium and high spatial resolution sources, respectively. This study involved matching the overpass time of these two satellites with the maps of EGs available in the study area, and matching the spectral ranges of the bands of these two satellites to calculate the used spectral indices, the high spatial resolution of Pléiades Neo satellite images in identifying EGs, and the appropriate spatiotemporal resolution. Compared to other satellite images available for free, such as Landsat and MODIS, Sentinel-2's matching ability and high efficiency of Sentinel satellite images in environmental science applications were the reasons for choosing these satellite images in this study.

Sentinel-2 imagery, with its bands offering resolutions of 10, 20, and 60 m and a revisit frequency of 6 days, was instrumental due to its optimal spatial, temporal, and spectral characteristics. For this study, the 10 m spectral bands were utilized, sourced from Sentinel Hub (https://www.sentinel-hub.com/, accessed on 5 May 2022). Pléiades Neo imagery (https://apollomapping.com/imagery/high-resolution-imagery; accessed on 28 April 2022), with a panchromatic resolution of 30 cm and a multispectral resolution of 120 cm, provided seven spectral bands, including Panchromatic, Deep Blue, Blue, Green, Red, Red Edge, and Near-infrared (NIR). The 26-day temporal resolution of this satellite facilitated the identification and measurement of EGs patterns, shapes, and sizes. Pan-sharpened multispectral bands from this satellite were employed to generate high-resolution spectral features, essential for EGs identification. Pansharpening is a technique used to enhance the spatial resolution of multispectral satellite bands by merging them with higher-resolution panchromatic imagery. The Intensity-Hue-Saturation (IHS) transform was used for pansharpening the Pléiades Neo imagery, combining the high spatial resolution of the panchromatic band with the spectral detail of the multispectral bands. This technique was selected due to its simplicity, computational efficiency, and ability to preserve spatial structures while minimizing spectral distortion. Compared to other approaches such as the Brovey transform, which can exaggerate spectral contrast and Gram–Schmidt fusion which requires more complex matrix operations and often introduces spectral artifacts in highly vegetated areas, the IHS method offers a good balance between spectral integrity and spatial enhancement, particularly for applications focusing on feature delineation like EG mapping. Moreover, IHS is well-suited for datasets with strong visible-band signals, making it an appropriate choice for the Pléiades Neo imagery used in this study. ENVI 5.3 software was used for pen sharpening process. The imagery was accessed from Apollo Mapping, with the Sentinel-2 and Pléiades Neo images dated 5 May 2022 and 28 April 2022, respectively.

3.2. Methods

The methodology encompassed three primary phases: generation of spectral features, implementation of EGs identification strategies, and accuracy assessment of the resultant EGs maps.

3.2.1. Generation of Effective Spectral Features

Spectral features were derived from the Blue, Green, Red, and NIR bands, common to both Pléiades Neo and Sentinel-2 imagery. These features, along with calculated spectral indices, were critical in distinguishing EGs from non-EG areas. Indices such as the normalized difference vegetation index (NDVI), Normalized Difference Water Index (NDWI), Norm NIR, Norm Red, Coloration index, Soil line, and Square Root (SQRT) were computed using established formulas (Table 1) [28–30]. To evaluate the statistical significance of differences in spectral feature values between EG and non-EG areas, two-sample *t*-tests were performed for each index. A RF model was employed to ascertain the variable importance measure (VIM) of these spectral features in EGs identification. Primary spectral features from Pléiades Neo imagery were initially at 0.6 m resolution, which were then upscaled to 2, 4, 6, and 8 m resolutions using averaging methods.

Table 1. Information of spectral indices used.

Index	Formula	Description
NDVI	$\frac{NIR-Red}{NIR+Red}$	The formation of EGs causes the loss of topsoil and consequently the loss of vegetation. Therefore, in the areas covered by EGs, the value of the NDVI is lower than non-EG areas.
NDWI	$\frac{Green-NIR}{Green+NIR}$	EGs are the result of washing and loss of soil. As a result, these areas are more concentrated than the areas around the EGs and the water accumulates in the EGs and the NDWI values in the places of EGs are higher than non-EGs in agricultural lands/farms.
Norm NIR	$\frac{NIR}{Red+Green+NIR}$	The values of the NIR band are influenced by the chlorophyll in the plants. Therefore, with the loss of vegetation due to the formation of EGs, the Norm NIR index values decrease. In the EGs areas, the values of this index are lower than the non-EGs areas. Also, the red band reflectance values are higher in areas without vegetation than in areas with vegetation. As a result, in agricultural areas, the values of the Norm Red index in EGs areas are higher than non-EGs areas.
Norm Red	$\frac{Red}{Red+Green+NIR}$	
Coloration index	$\frac{Red-Blue}{Red}$	Coloration index is calculated based on red and blue bands. The values of this index in EGs areas are higher than non-EGs areas in agricultural lands/farms.
Soil line	$NIR - 2.4Red$	EGs is a phenomenon related to soil. Also, EGs formation affects the vegetation. Considering that in the calculation of Soil line and SQRT index, two NIR and Red bands related to vegetation and soil information are used, they can be effective in identifying EGs. The type of spectral behavior of NIR and Red bands in soil and plant covers causes Soil line and SQRT index values to be different in EGs areas from non-EGs areas.
SQRT	$\sqrt{\frac{NIR}{Red}}$	

3.2.2. EGs Identification Strategies

Three distinct strategies, all utilizing the RF algorithm, were implemented for EGs mapping at various spatial resolutions. The first strategy involved calibrating a predictive model with Sentinel-2 derived spectral features, producing EGs maps at 10 m resolution (Figure 2). In this strategy, effective spectral feature maps were first produced using Sentinel-2 images with a resolution of 10 m. Then, the values of these features were extracted from the 10 m maps obtained from Sentinel-2 in the geographic location of the samples dataset. The extracted values are used as training samples in the RF model. After building the model, using these training samples, and applying it to the maps of spectral features obtained from Sentinel-2 images, a 10 m EGs map was prepared.

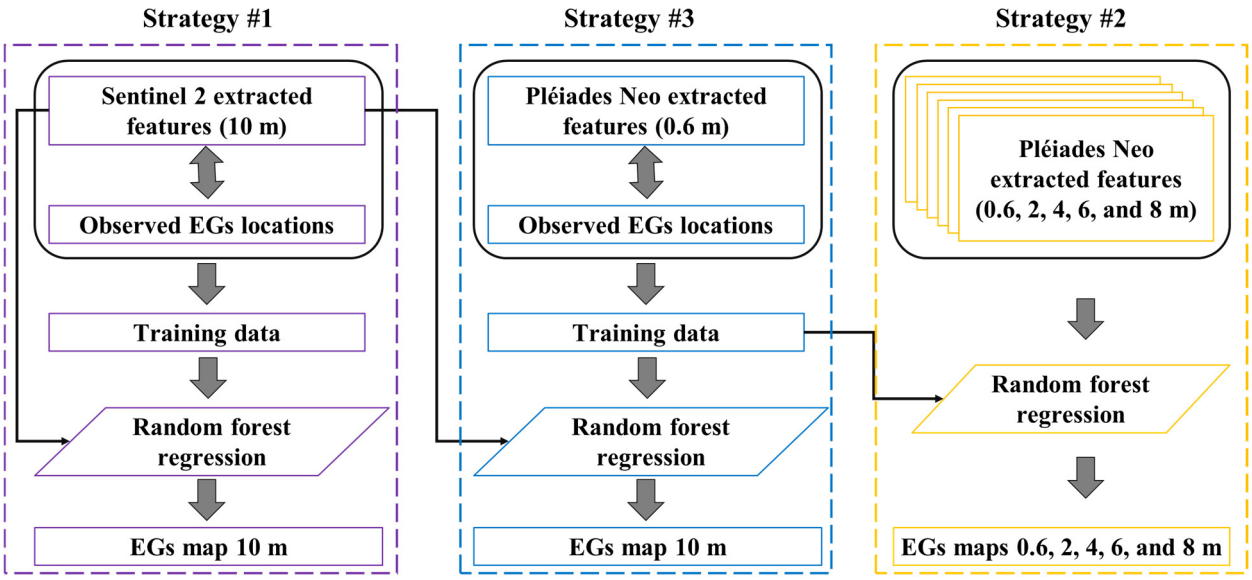

Figure 2. Conceptual model of strategies used for EGs identification.

The second strategy utilized high-resolution (0.6 m) Pléiades Neo data for model development, with subsequent application across different resolutions (0.6, 2, 4, 6, and 8 m), assessing the impact of spatial resolution on EGs identification accuracy. In this strategy, effective spectral feature maps with a spatial resolution of 0.6 m were first generated from the Pléiades Neo image. Then, using the nearest neighbor resampling method, spectral feature maps were prepared with spatial resolutions of 2, 4, 6, and 8 m. Then, for the geographic location of the sample dataset, the values of the effective spectral features were extracted from the 2, 4, 6, and 8 m maps obtained from the Pléiades Neo image. Separately, the RF model was calibrated based on the sampling datasets prepared at each spatial resolution and applied to the spectral feature maps of the same spatial resolution. Finally, EGs maps with a spatial resolution of 2, 4, 6, and 8 m were prepared based on this strategy.

The third strategy applied the high-resolution calibrated model (from Pléiades Neo data) to Sentinel-2 imagery, generating 10 m resolution EGs maps (upscaling strategy). In this strategy, the calibrated RF model was used based on the sampling dataset obtained from the 0.6 m maps in the second strategy to prepare the EGs map. This model was applied on the 10 m spectral feature maps obtained from Sentinel-2 images, and the output is an EG map with a resolution of 10 m.

3.2.3. Predictive Modeling Using Random Forest

The RF algorithm, a robust machine learning method, was employed for predictive modeling [31]. This approach integrates multiple decision trees, with each tree corresponding to a randomly and independently sampled vector. RF is one of the most widely used machine learning algorithms in environmental modeling [32]. The advantages of this algorithm are: (1) adding or subtracting parameters without restrictions based on information access and purpose, (2) limiting the number of parameters that must be defined by the user, (3) calculating the variable importance and contribution of each independent variable in the final model automatically, (4) the ability to model complex and non-linear relationships between independent and dependent variables, and (5) the ability to simultaneously consider continuous and categorical parameters. Different indices and spectral bands are effective in identifying EGs, and the type and degree of effectiveness of each of them is different and complex. As a result, the use of RF algorithm can be effective in identifying EGs.

The RF model was calibrated to define the relationship between the dependent variable (EGs presence) and independent variables (nine spectral features). A total of 367 EG pixels

and 346 non-EG pixels were randomly selected from visually interpreted ground-truth data and used to train the Random Forest model. This sample size was found to be sufficient to capture the spectral variability of both classes across the study area and is consistent with similar studies on gully detection. To prevent overfitting and ensure the generalizability of the model, we adopted a train-test split strategy. The selected samples were used exclusively for model training, while an independently generated ground-truth map of actual EGs in the study area was used for model testing and accuracy evaluation. This independent validation approach provides a realistic assessment of the model's performance in operational settings. The values of 9 spectral indices were extracted in the geographical location of the samples in order to make a connection between these spectral features and EGs presence using the RF model. Then, the built model was used to calculate the probability of EGs occurrence in pixels other than the sample pixels in the study area. For this purpose, the probability was calculated by different decision trees generated by the RF model. The final EGs probability map was derived from the aggregated probabilities across all decision trees.

The same modeling structure was applied across all three strategies, with the main differences being the source and resolution of the spectral features:

- Strategy 1 (Direct Sentinel-2): RF model trained and applied using 10 m spectral features derived from Sentinel-2 imagery.
- Strategy 2 (Multi-resolution Pléiades Neo): RF model trained using high-resolution (0.6 m) Pléiades Neo features, and applied to resampled datasets at 2, 4, 6, and 8 m resolutions.
- Strategy 3 (Upscaling): RF model trained on 0.6 m Pléiades Neo features and applied to 10 m Sentinel-2 imagery.

In all cases, the trained model was applied to the full image to generate probability maps of EG presence.

3.2.4. Accuracy Assessment

To convert the probability maps generated by the Random Forest model into binary classifications of EG and non-EG, a threshold value needed to be defined. A range of thresholds from 0.40 to 0.95 was evaluated in 0.05 increments. For each value, the classification results were compared against the ground-truth EG map using standard accuracy metrics, including overall accuracy and the user's and producer's accuracy. The threshold of 0.85 was ultimately selected because it minimized the overall classification error while maintaining a balance between omission and commission errors. This value provided the best alignment with field-verified EG patterns and produced consistent results across different resolution scenarios. Error maps for each strategy were generated by overlaying predicted EGs maps with field-verified EGs maps. The effectiveness of each strategy was evaluated using metrics such as omission and commission errors, calculated using Equations (1) and (2). Additionally, the sensitivity of EGs identification accuracy relative to spatial resolution was investigated by comparing errors across different strategies.

$$OE = \frac{N}{G} \tag{1}$$

$$CE = \frac{M}{NG} \tag{2}$$

Additionally, a one-way analysis of variance (ANOVA) was conducted to compare overall classification errors among the three EG mapping strategies. Where appropriate, post hoc Tukey tests were applied to identify significant pairwise differences. All statistical analyses were conducted using R software, with a significance level set at $p < 0.05$.

4. Results

4.1. Effective Spectral Features Maps

The maps of spectral features (0.6 m) derived from Pléiades Neo affecting the EGs identification are shown in Figure 3. Visual examination of the maps showed that the values of these features were different in EGs and non-EGs area. Due to continuous soil erosion and water accumulation in EGs area, the amount of vegetation and greenness was lower than in non-EGs areas; as a result, the values of NDVI and Norm-NIR in EGs were lower than in non-EGs area. Due to higher moisture in areas located in EGs, the value of NDWI in these areas was higher than non-EGs areas. In general, the values of Red band, NIR band, NDVI, Norm_NIR, Soil line, and SQRT in EGs areas were lower than non-EGs areas. But the values of NDWI, Norm_Red, and Coloration Index in EGs area were higher than non-EGs area. The mean values of NIR band, Red band, NDVI, NDWI, Norm_Red, Norm_NIR, Soil line, SQRT, and Coloration Index for non-EGs area were 0.07, 0.12, 0.71, 0.32, 0.18, 0.34, 0.67, 0.49, and 0.34, respectively (Table 2). These values for the EGs area were 0.05, 0.10, 0.68, 0.34, 0.23, 0.22, 0.66, 0.46, and 0.40, respectively. The standard deviation (SD) of all spectral features in EGs area was lower than in non-EGs area, which indicates the higher heterogeneity of spectral features values in non-EGs area compared to EGs area. To determine whether the differences in spectral feature values between EG and non-EG areas were statistically significant, two-sample *t*-tests were conducted for each index. The results showed that indices differed significantly between the two classes, supporting their suitability for EG detection.

Table 2. Statistical parameters of spectral features values in EGs and non-EGs regions.

Effective Spectral Features		Minimum	Maximum	Range	Mean	Standard Deviation
Red	Non-Gully	0	1	1	0.071	0.010
	Gully	0.019	0.141	0.122	0.058	0.009
NIR	Non-Gully	0	1	1	0.1265	0.018
	Gully	0.022	0.237	0.214	0.100	0.018
NDVI	Non-Gully	0	0.996	0.997	0.711	0.027
	Gully	0.423	0.944	0.521	0.680	0.025
NDWI	Non-Gully	0	1	1	0.323	0.028
	Gully	0.060	0.624	0.565	0.343	0.026
Norm Red	Non-Gully	0	1	1	0.186	0.041
	Gully	0.060	0.514	0.454	0.233	0.042
Norm NIR	Non-Gully	0	0.998	0.998	0.244	0.035
	Gully	0.092	0.730	0.638	0.228	0.021
Soil line	Non-Gully	0	0.990	0.990	0.672	0.020
	Gully	0.547	0.897	0.350	0.662	0.013
Coloration index	Non-Gully	0	1	1	0.344	0.057
	Gully	0.174	0.701	0.527	0.408	0.053
SQRT	Non-Gully	0	0.990	0.990	0.499	0.033
	Gully	0.262	0.852	0.591	0.467	0.028

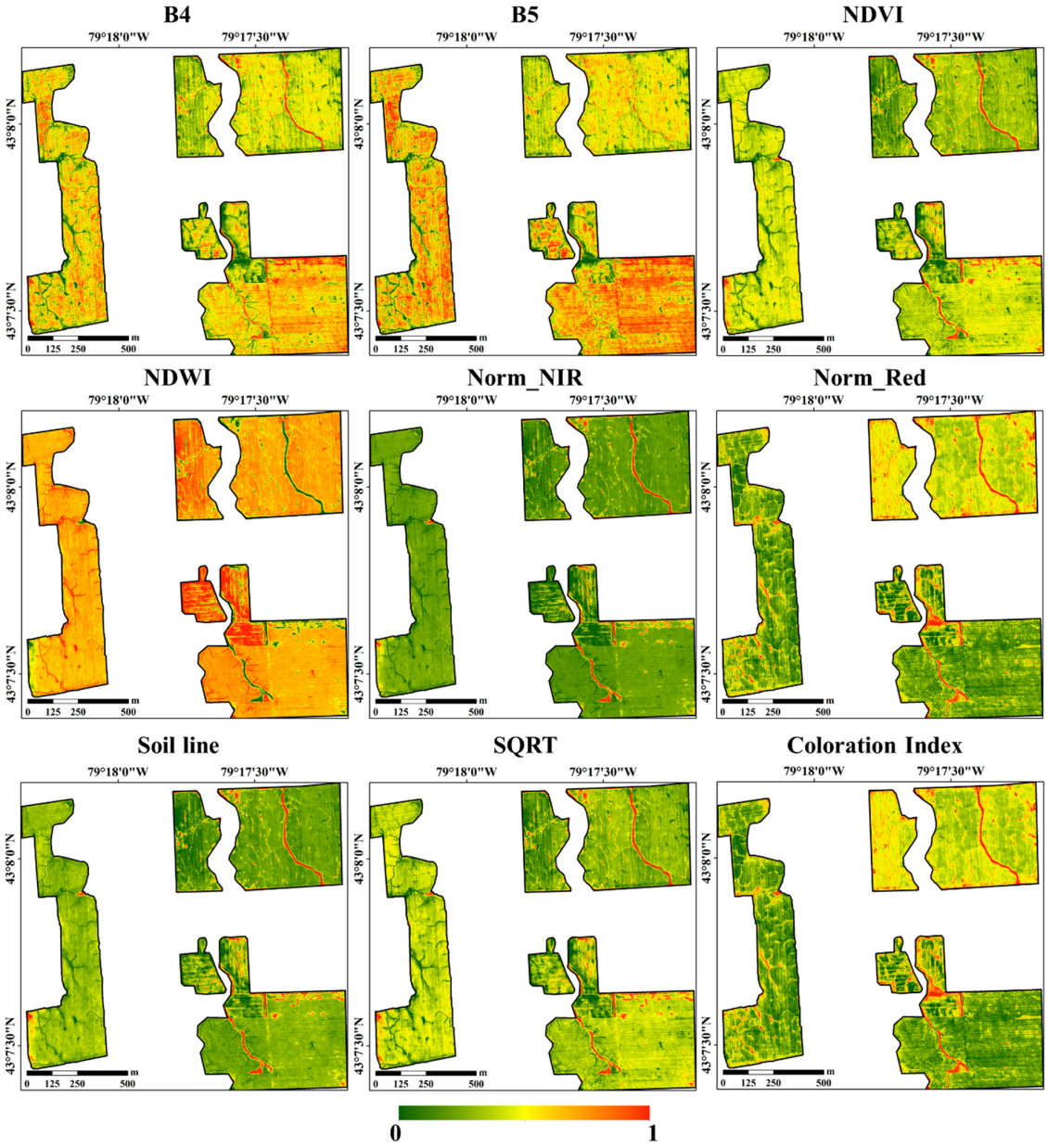

Figure 3. Maps of spectral features used in the prediction of EGs. (The values of 1 (red color) on the maps indicate the highest values of the spectral features and the values of 0 (green color) indicate the lowest values of the spectral features).

4.2. Effective Spectral Features Importance Degree

The mean values for each of the spectral features used to predict the occurrence of EGs differed when comparing EGs to non-EGs in the study area. This was reflected in the VIM extracted from the calibrated RF model. The mean VIM of each of these spectral features obtained from different sources (Sentinel-2 and Pléiades Neo) for EGs identification was shown in Figure 4. The VIM of Norm_NIR, Soil line, NDVI, NDWI, Coloration Index, SQRT, NIR, Red, and Norm_Red were 18, 15, 12, 10, 9, 9, 8, 5, and 3%, respectively. Norm NIR and Norm Red had the highest and lowest VIM, respectively. The VIM of the spectral features related to vegetation was higher than the surface wetness related spectral features. The mean spectral indices VIM (10.6%) in identifying EGs was higher than the VIM of spectral bands (6.5%).

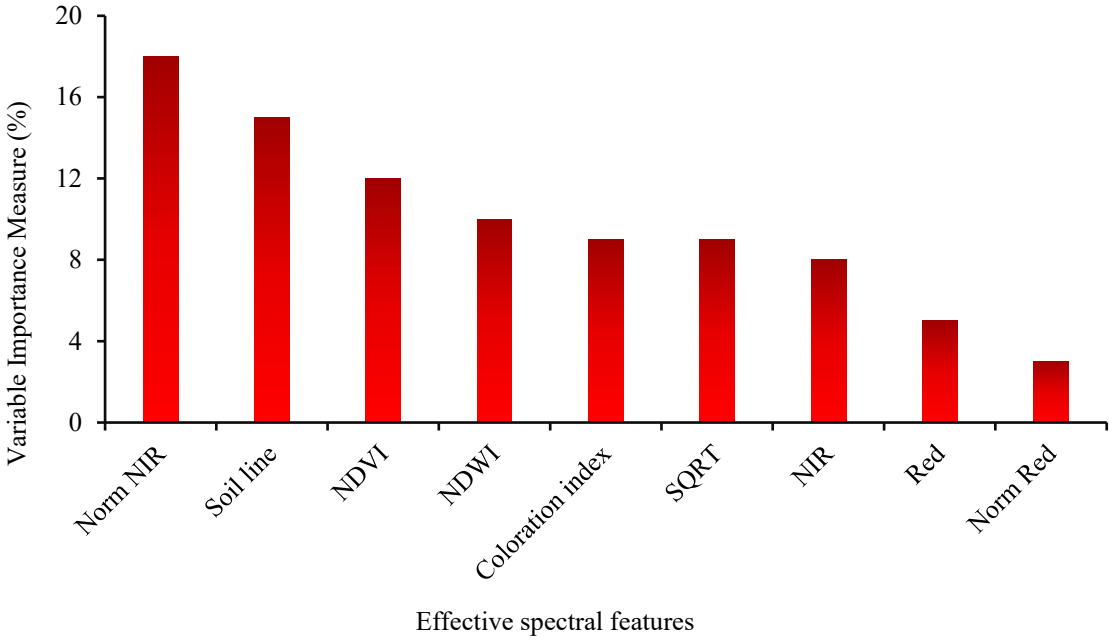

Figure 4. The Variable Importance Measure (VIM) of the spectral features used in the identification of EGs.

4.3. EGs Occurrence Probability Maps

Maps depicting the probability of occurrence of EGs at different spatial resolutions were shown in Figure 5. The spatial distribution of areas with a high probability for the presence of EGs was varied across the different maps. The average probability for the occurrence of EGs for the study area at spatial resolutions of 0.6, 2, 4, 6, 8, and 10 m (upscaling strategy) were 0.26, 0.24, 0.23, 0.21, 0.19, and 0.18, respectively. With the increase in the spatial resolution, the average probability of the occurrence of EGs based on the upscaling strategy decreases. In maps with higher spatial resolution, higher details of the probability of occurrence of EGs can be displayed. In maps with lower spatial resolution, lower probability values have been calculated for the corresponding geographic location of small EGs compared to higher spatial resolution. The average value of the probability of occurrence of EGs based on the model obtained from Sentinel-2 images (direct strategy) with a spatial resolution of 10 m was 0.36, which is higher than the values obtained based on the upscaling strategy, which shows that the calibrated model based on Sentinel-2 data was more optimistic than the upscaling strategy in identifying EGs.

The mean and SD of the probability of occurrence of EGs in the geographical location of observed EGs (non-EGs) based on upscaling strategy for the spatial resolutions of 0.6, 2, 4, 6, 8, and 10 m, were 0.79 (0.19), 0.77 (0.18), 0.76 (0.17), 0.74 (0.16), 0.71 (0.16), and 0.68 (0.15), respectively (Figure 6). With the increase in the spatial resolution, the calculated mean for the potential in the geographical location of the observed EGs in the study area decreased which indicates a lower probability of identifying the EGs in low spatial resolutions. These values were 0.31 and 0.72 in EGs and non-EGs areas for the calibrated model based on Sentinel-2, respectively. The mean potential difference between the observed EGs and observed non-EGs locations at a spatial resolution of 10 m based on the upscaling strategy and the calibrated model based on Sentinel-2 were 0.53 and 0.41, respectively. These results showed that the ability of the calibrated model based on Sentinel-2 in identifying EGs was lower than the upscaling strategy.

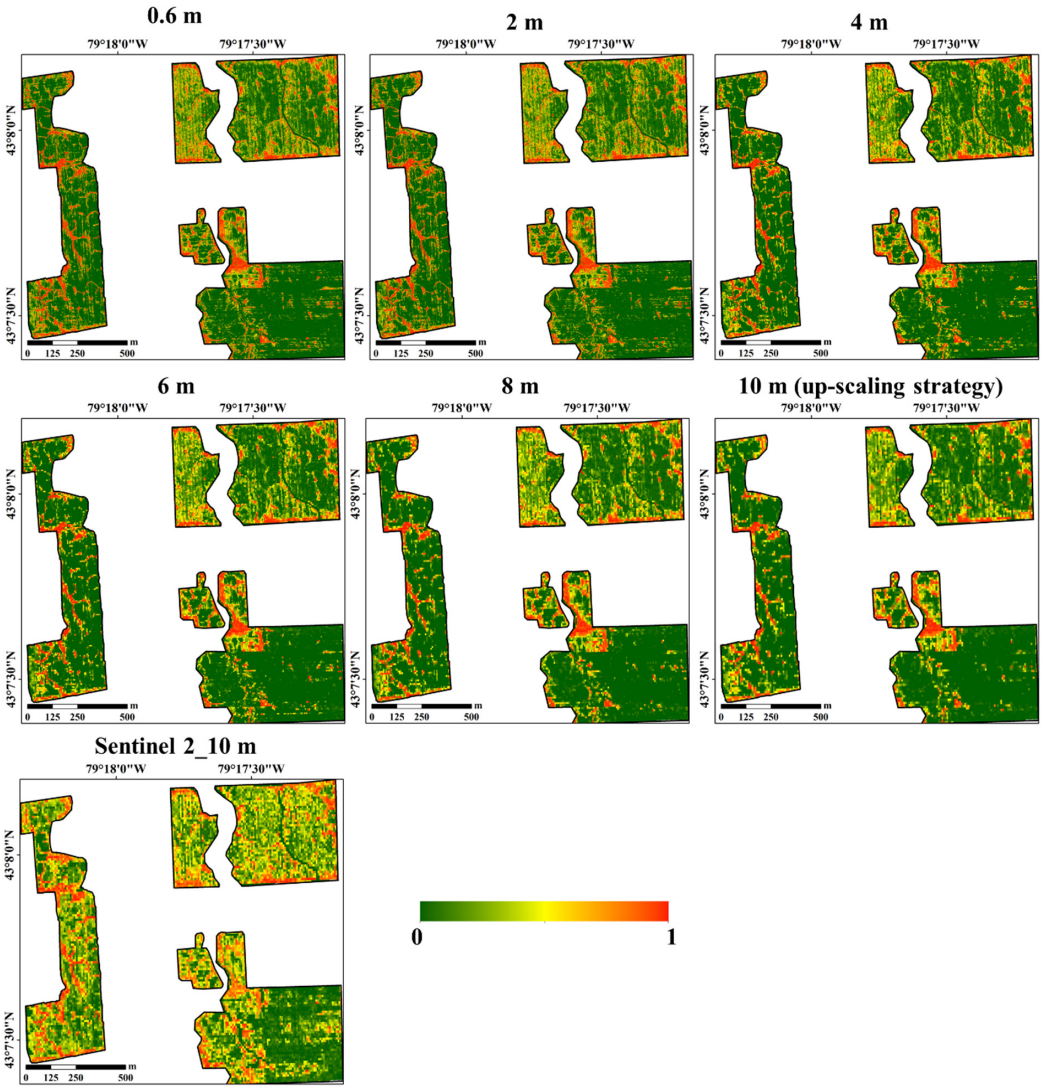

Figure 5. Maps depicting the probability of occurrence of EGs generated based on 0.6, 2, 4, 6, 8, and 10 m spatial resolution (upscaling strategy) and 10 m (calibrated model based on Sentinel-2 data; direct strategy) (the values of 1 (red color) on the maps indicate the highest probability of occurrence of EGs and the values of 0 (green color) indicate the lowest probability of occurrence of EGs).

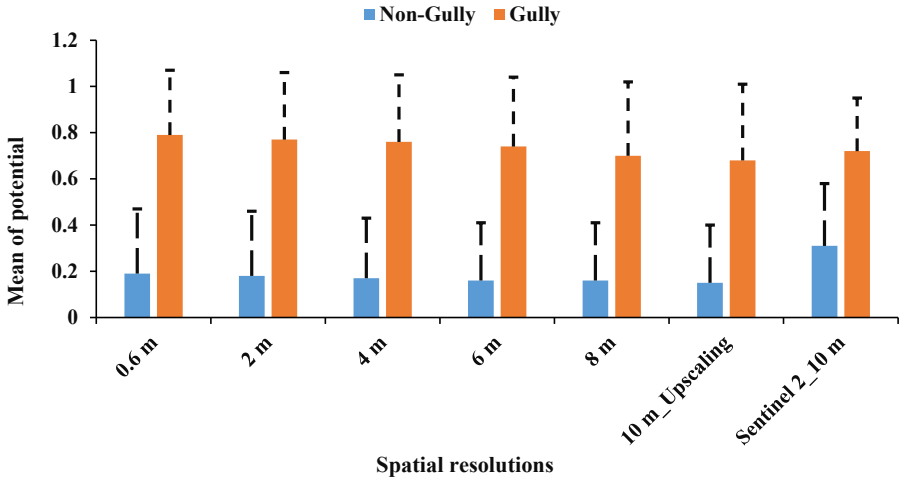

Figure 6. The mean and standard deviation (SD) of the potential for the EGs occurrence in the geographical location of observed EGs and non-EGs areas.

4.4. Identified EGs Maps

By determining the appropriate threshold value, EGs maps for the study area were prepared based on each strategy and shown in Figure 7. The area of EGs identified based on upscaling strategy for spatial resolution of 0.6, 2, 4, 6, 8, and 10 m (upscaling strategy) were 0.143, 0.141, 0.12, 0.113, 0.108, and 0.105 km^2, respectively. With increasing spatial resolution, less area has been identified as EGs. The difference in these values with the observed value of EGs were 0.064, 0.062, 0.041, 0.034, 0.029, and 0.026 km^2 respectively. The area of EGs detected using calibrated model based on Sentinel-2 was 0.153, which was more than the observed value of EGs about 0.075 km^2. In this strategy, more areas were identified as EGs than the upscaling strategy, and it had lower accuracy in terms of the amount of identified EGs area.

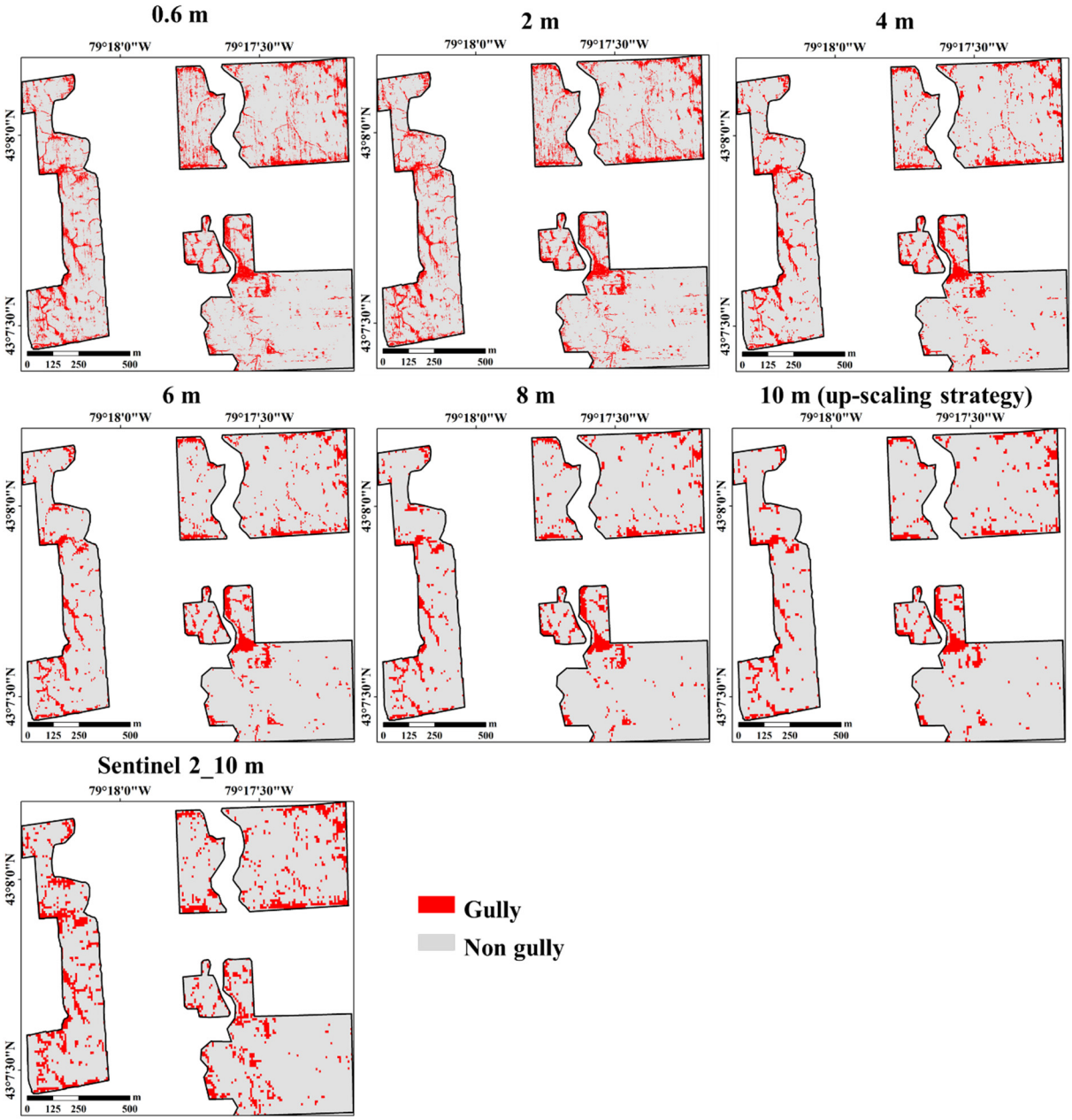

Figure 7. EGs maps for the study area prepared based on upscaling strategy for spatial resolution of 0.6, 2, 4, 6, 8, and 10 m and the calibrated model based on Sentinel-2.

4.5. Spatial Accuracy Assessment

The spatial accuracy assessment maps for different strategies including the location of identified, unidentified and incorrectly identified EGs are shown in Figure 8. The area of the "EGs identified correctly" in the prepared maps based on the up-scaling strategy in spatial resolution of 0.6, 2, 4, 6, 8, and 10 m were 0.057, 0.056, 0.053, 0.051, 0.048, and 0.045, respectively. This amount for the calibrated model based on Sentinel-2 was also 0.044 km^2, which was a lower value than the upscaling strategy. Also, the area of "non-EGs incorrectly classified in the EGs class" in the maps obtained from the up-scaling strategy in spatial resolution of 0.6, 2, 4, 6, 8, and 10 m and the calibrated model based on Sentinel-2 were 0.086, 0.084, 0.065, 0.061, 0.059, 0.058, and 0.118 km^2, respectively. From this point of view, the upscaling strategy has a higher efficiency than the calibrated model based on Sentinel-2. By increasing the spatial resolution in the upscaling strategy, the amount of non-EGs area classified as the EGs class was reduced incorrectly. On the other hand, the examination of the spatial accuracy assessment map showed that 0.021, 0.022, 0.024, 0.026, 0.029, 0.031, and 0.032 km^2 of EGs were incorrectly classified as the non-EGs class based on these strategies, respectively. One-way ANOVA was performed to assess whether the overall classification errors differed significantly across the mapping strategies. The results indicated a statistically significant difference ($p < 0.01$), confirming that the upscaling strategy significantly outperformed the direct Sentinel-2 approach in terms of accuracy. Post hoc Tukey tests further revealed that the improvement was most pronounced at 10 m resolution.

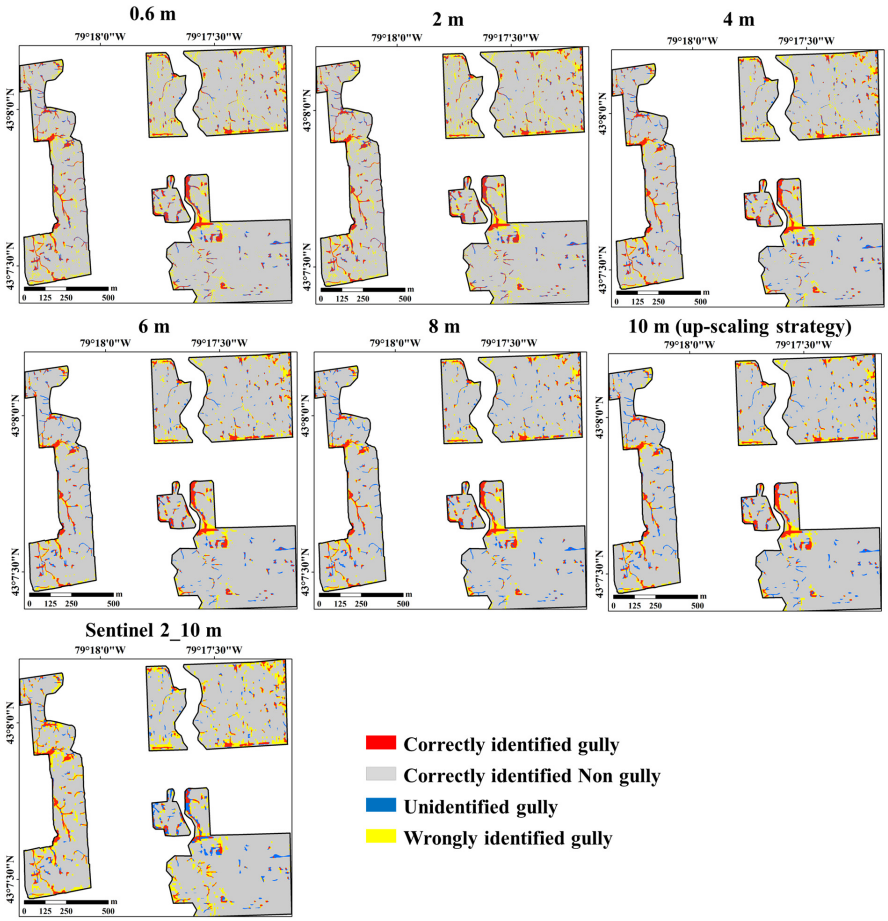

Figure 8. Spatial accuracy evaluation maps for upscaling strategy with spatial resolution of 0.6, 2, 4, 6, 8, and 10 m and calibrated model based on Sentinel-2.

The results of the accuracy assessment for the upscaling strategy for spatial resolution of 0.6, 2, 4, 6, 8, and 10 m and the calibrated model based on Sentinel-2 to identify the EGs were shown in Figure 9. The omission error of the upscaling strategy in spatial resolution of 0.6, 2, 4, 6, 8, and 10 m and the calibrated model based on Sentinel-2 were 27.8, 28.7, 31.4, 34.5, 38.7, 42.3, and 44.2%, respectively. These results show that by increasing the spatial resolution, the number of undetected EGs should be significantly reduced. The error of the EGs identification using the calibrated model based on Sentinel-2 was higher than the upscaling strategy in the spatial resolution of 10 m. The commission error for these models was 8.9, 8.7, 6.8, 6.3, 6.1, 6.0, and 11.9%, respectively. In the calibrated model based on Sentinel-2, a significant number of lands identified as EGs were actually non-EGs areas, if using the upscaling strategy, the error of classifying non-EGs areas into EGs in the spatial resolution was 10 m decreased significantly. The overall error showed that the best result related to spatial resolution was map with spatial resolution of 0.6 m. By decreasing the spatial resolution, the identification error was increased, but by using the proposed upscaling strategy instead of calibrated model based on Sentinel-2, the accuracy of EGs identification at low spatial resolution can be significantly increased.

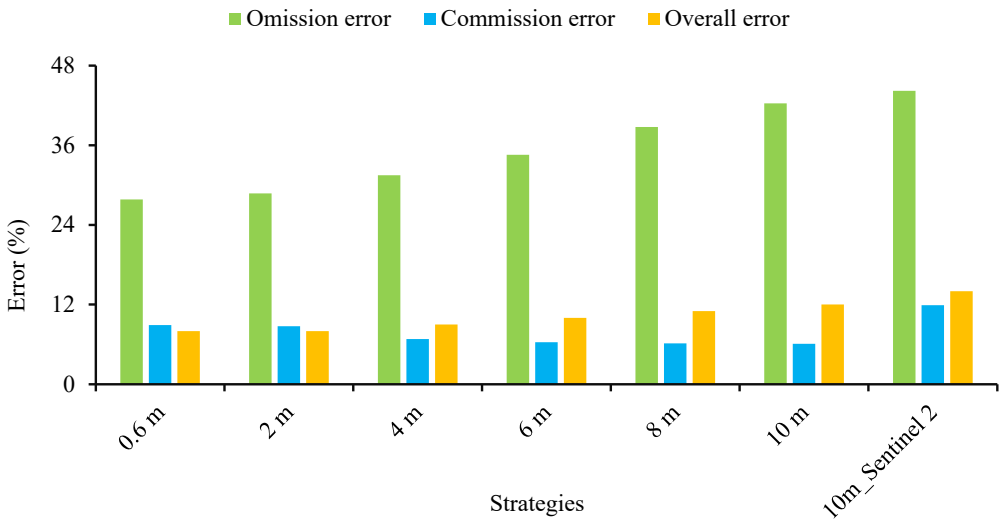

Figure 9. Accuracy assessment of the three EGs identification strategies, showing omission error, commission error, and overall classification error.

5. Discussion

5.1. Complexities and Variabilities in EGs Identification

The identification of EGs presents unique challenges due to their rapid variability and smaller size compared to permanent gullies. This study's exploration of various strategies underscores that the accuracy of EGs identification is influenced by multiple factors. These include the spatial resolution of predictors, the structure of training models, and the nature of the features used [14,22,33]. The type of features, whether biophysical or topographical, and their spatial resolution play a crucial role in the accuracy of EGs identification [34,35]. Given the limited availability of time-series topographic data for many regions, this study pivoted towards an independent model focusing on spectral features, including bands and indices, which can be extracted from satellite images of varying resolutions. These images, available in time series, offer a more accessible alternative to topographic data [33,36,37].

5.2. Integrated Role of Spectral Features and Spatial Resolution in EGs Mapping

Although EGs are primarily influenced by topographic processes, this study demonstrates that spectral features particularly those related to vegetation cover and surface

wetness are highly effective for their identification. Indices such as NDVI and Norm NIR showed strong relevance, likely due to the contrast in reflectance patterns between disturbed gully areas and surrounding vegetation. This supports findings from prior studies indicating that spectral data can supplement or even substitute for topographic variables in EG mapping [33,36,37].

In parallel, spatial resolution emerged as a key determinant of mapping accuracy. High-resolution imagery, especially Pléiades Neo at 0.6 m, consistently outperformed medium-resolution data in detecting narrow and shallow EG features [38–40]. However, such imagery is limited by high acquisition costs and lower revisit frequency, constraining its use in large-scale, repeated applications. In contrast, medium-resolution data like Sentinel-2 offer global coverage and open access, making them suitable for operational implementation if model performance can be enhanced.

The proposed upscaling strategy bridges this gap by calibrating the model on high-resolution data and applying it to coarser imagery. This approach yielded lower classification errors compared to direct Sentinel-2 modeling, confirming that leveraging fine-scale information can improve the performance of medium-resolution EG mapping. Ultimately, accurate and scalable EG identification depends on both selecting effective spectral features and intelligently managing spatial resolution.

The performance of the proposed upscaling strategy aligns well with or exceeds that reported in recent EG mapping studies. For example, Liu et al. [22] achieved an overall classification accuracy of approximately 87% using a deep learning model applied to high-resolution UAV imagery in a small region of the Loess Plateau. While their approach benefited from ultra-fine resolution and intensive ground truthing, its applicability is limited in larger-scale settings due to computational and logistical demands. Similarly, Wang et al. [24] used hybrid models to predict gully erosion susceptibility with accuracies ranging from 82% to 88%, also within localized watersheds. In contrast, our approach achieved an overall accuracy of 87.5% at 10 m resolution using the upscaling strategy, demonstrating competitive performance while using freely available medium-resolution imagery. This comparison highlights the value of the upscaling approach in achieving scalable, accurate, and resource-efficient EG detection over large agricultural landscapes.

5.3. Model Training and Upscaling Strategy

A key aspect of developing an accurate EGs identification model is the training process. As spatial resolution decreases, the heterogeneity within a pixel increases, potentially elevating model error when using low-resolution data for training. This study advocates for a model trained with high-resolution data, subsequently applied to medium-resolution satellite imagery. The results demonstrate that this upscaling strategy significantly enhances the accuracy of models based on moderate-resolution satellite data. This approach offers a viable solution for EGs identification across extensive agricultural landscapes, leveraging the widespread availability of satellite imagery.

Although the upscaling strategy improved EG mapping accuracy compared to the direct Sentinel-2 model, some classification errors remained. Several factors may have contributed to these inaccuracies. First, temporal discrepancies between the acquisition dates of Pléiades Neo and Sentinel-2 imagery may have introduced differences in surface conditions, especially vegetation cover or soil moisture. Second, minor cloud shadows or variations in illumination could have affected the spectral signatures of EGs. Third, pansharpening artifacts particularly edge enhancement effects introduced by the IHS method may have altered the spectral integrity of some high-resolution pixels. Lastly, certain non-EG features (e.g., field boundaries or furrows) may have spectral characteristics similar to EGs, leading to misclassification.

5.4. Integrated Impacts and Implications

The outcomes of this study have significant implications that transcend the technical aspects of EGs mapping, impacting broader environmental and agricultural management domains. The adoption of an upscaling strategy for EGs identification marks a pivotal advancement in soil conservation and sustainable land management practices. This approach aligns with the principles outlined by Pimentel [41] and Lal [42], who emphasize the critical need for accurate soil erosion assessment to safeguard soil health and agricultural productivity. Accurate mapping and monitoring of EGs, especially over extensive areas, are instrumental in enhancing our ability to predict and mitigate soil erosion. This is in line with the findings of [43], who highlights the importance of understanding soil erosion dynamics for sustainable land use planning. By facilitating precise EGs identification, this research supports the maintenance of soil integrity, which is essential for agricultural productivity and ecological balance, as discussed by Lal [44] and Foley et al. [45]. Moreover, the methodology employed in this study, leveraging accessible satellite data, offers a scalable and cost-effective approach to soil and water conservation. This aspect is particularly relevant in the context of global environmental challenges, as noted by [46,47], who advocate for innovative, data-driven solutions in environmental management. The implications of this research extend to informing policy decisions and practical interventions in precision agriculture and environmental stewardship. The integration of satellite-based EGs mapping into agricultural management practices can significantly contribute to the goals of sustainable agriculture, as described by [48,49]. In essence, this study not only enhances our understanding of EGs dynamics but also offers a pragmatic pathway for addressing some of the pressing challenges in soil conservation and agricultural sustainability [41–43,45,46,49].

5.5. Limitations and Future Directions

This study acknowledges several limitations that warrant further investigation and refinement in future work. First, the ephemeral nature of gullies poses a major challenge for consistent detection, as EGs often appear only after intense rainfall or tillage and may disappear shortly after. To address this, future studies should incorporate multi-temporal imagery (e.g., time series from Sentinel-2 or PlanetScope) to better capture the short-lived dynamics of EGs and identify optimal observation windows based on seasonality, land use, and climatic conditions. Second, although high-resolution imagery significantly enhances mapping accuracy, its acquisition remains costly and often infeasible for repeated, large-scale monitoring. A practical solution is to calibrate models using high-resolution data from limited sites, then apply them to medium-resolution imagery (e.g., Sentinel-2, Landsat 8/9) through upscaling. This approach, demonstrated in our study, mitigates dependence on costly data and enables broader coverage. Third, computational intensity is a key constraint when processing large-scale imagery and training ensemble models like Random Forest. This can be addressed by adopting cloud-based platforms such as Google Earth Engine or Amazon Web Services, which allow scalable and efficient model training, prediction, and analysis over wide areas. Another challenge is the spectral confusion between EGs and similar landscape features such as rills, field furrows, or natural drainage lines. Future studies could integrate contextual spatial features, or combine optical data with LiDAR or radar sources, to improve structural differentiation. While field-based EG detection methods are accurate, they are limited in spatial coverage and resource-intensive. Compared to these traditional techniques, the upscaling strategy proposed here offers a scalable, efficient alternative by combining the spectral sensitivity of high-resolution models with the accessibility of medium-resolution imagery. This hybrid approach reduces costs and operational limitations while preserving mapping accuracy. Finally, the current study was constrained by the lack of real EG maps from other regions, limiting model

generalization. Future research should validate the transferability of upscaling models to new geographic contexts and assess their robustness across varying soil types, climates, and land management systems.

6. Conclusions

This study proposed an upscaling-based strategy to enhance the mapping accuracy of EGs using freely available medium-resolution satellite imagery. By calibrating a machine learning model with high-resolution data and applying it to Sentinel-2 imagery, we demonstrated that it is possible to overcome spatial resolution limitations without compromising mapping performance. Beyond methodological innovation, this approach offers a practical solution for large-scale soil erosion monitoring in agricultural landscapes. The upscaling technique can be integrated into existing farm management systems and GIS-based land monitoring platforms to support sustainable soil conservation practices. Its reliance on globally accessible data, combined with its scalability, makes it particularly well-suited for operational use in regions where high-resolution imagery is either unavailable or unaffordable. This research contributes not only to remote sensing methodology but also to broader goals in land degradation mitigation, environmental planning, and agricultural resilience. By improving EG detection accuracy, stakeholders can better identify vulnerable zones, implement targeted erosion control measures, and optimize land use strategies. Future research should focus on testing the proposed approach across varied agroecological zones and under different climatic and management conditions. Additionally, incorporating multi-temporal satellite imagery could improve the detection of short-lived EG features and help track their evolution over time. Expanding the model's applicability to diverse landscapes will further enhance its robustness and practical utility.

Author Contributions: Conceptualization, A.B., P.D. and S.F.; methodology, S.F. and D.D.S.; software, S.F. and D.D.S.; validation, S.F. and D.D.S.; formal analysis, S.F.; data curation, S.F., H.S.M., N.K., H.B.V., M.N. and S.F.; writing—original draft preparation, S.F.; writing—review and editing, A.B., P.D. and D.D.S.; supervision, A.B. and P.D.; project administration, A.B. and P.D.; funding acquisition, P.D. and A.B. All authors have read and agreed to the published version of the manuscript.

Funding: This research was funded by Ontario Agri-Food Alliance Tier 1 Program (PI Prasad Daggupati, Co-PI- Asim Biswas), Grant number [UG-T1-2021-101129] and Natural Sciences and Engineering Research Council (PI- Asim Biswas), Grant number [RGPIN-2020-05017]. The APC was also funded by Natural Sciences and Engineering Research Council, Grant number [RGPIN-2020-05017].

Data Availability Statement: The data used to support the findings of this study are available from the corresponding author upon reasonable request.

Conflicts of Interest: The authors declare no conflicts of interest.

References

1. Castillo, C.; Gómez, J. A century of gully erosion research: Urgency, complexity and study approaches. *Earth-Sci. Rev.* **2016**, *160*, 300–319. [CrossRef]
2. Dai, W.; Hu, G.-h.; Yang, X.; Yang, X.-w.; Cheng, Y.-h.; Xiong, L.-y.; Strobl, J.; Tang, G.-a. Identifying ephemeral gullies from high-resolution images and DEMs using flow-directional detection. *J. Mt. Sci.* **2020**, *17*, 3024–3038. [CrossRef]
3. Kang, H.; Guo, M.; Wang, W. Ephemeral gully erosion in concentrated flow channels induced by rainfall and upslope inflow on steep loessial slopes. *Land Degrad. Dev.* **2021**, *32*, 5037–5051. [CrossRef]
4. Ollobarren, P.; Capra, A.; Gelsomino, A.; La Spada, C. Effects of ephemeral gully erosion on soil degradation in a cultivated area in Sicily (Italy). *Catena* **2016**, *145*, 334–345. [CrossRef]
5. Wilson, G.; Wells, R.; Dabney, S.; Zhang, T. Filling an ephemeral gully channel: Impacts on physical soil quality. *Catena* **2019**, *174*, 164–173. [CrossRef]
6. Xu, X.; Zheng, F.; Tang, Q.; Wilson, G.V.; Wu, M.; Han, Y.; Xiao, P.; Zhang, X.J. Upslope sediment-laden flow impacts on ephemeral gully erosion: Evidences from field monitoring and laboratory simulation. *Catena* **2022**, *209*, 105802. [CrossRef]

7. Wells, R.R.; Momm, H.G.; Bennett, S.J.; Gesch, K.R.; Dabney, S.M.; Cruse, R.; Wilson, G.V. A measurement method for rill and ephemeral gully erosion assessments. *Soil Sci. Soc. Am. J.* **2016**, *80*, 203–214. [CrossRef]
8. Tang, J.; Liu, G.; Xie, Y.; Duan, X.; Wang, D.; Zhang, S. Annual variation of ephemeral gully erosion in a cultivated catchment. *Geoderma* **2021**, *401*, 115166. [CrossRef]
9. Daggupati, P.; Roy, S.; Mckague, K.; Patterson, C.; Biswas, A. Simulating Ephemeral Gully Erosion Using AnnAGNPS in Agricultural Fields of Southern Ontario, Canada. In Proceedings of the EGU General Assembly Conference Abstracts, Vienna, Austria, 8–13 April 2018; p. 13703.
10. Ireland, H.A.; Eargle, D.H.; Sharpe, C.F.S. *Principles of Gully Erosion in the Piedmont of South Carolina*; US Department of Agriculture: Washington, DC, USA, 1939.
11. Moore, I.; Burch, G.; Mackenzie, D. Topographic effects on the distribution of surface soil water and the location of ephemeral gullies. *Trans. ASAE* **1988**, *31*, 1098–1107. [CrossRef]
12. Porta, J.; Ramos, J.; Boixadera, J. Mechanical measures for runoff management and erosion control in the vineyards of north east Spain. In *Conserving Soil Resources: European Perspectives*; Selected papers from the First International Congress of the European Society for Soil Conservation; CAB International: Wallingford, UK, 1994; pp. 369–378.
13. Shi, H.; Xiao, H.; Liu, G.; Abd Elbasit, M.A.; Zheng, F.; Zhang, Q.; Zhang, Y.; Guo, Z. Identifying interrill, rill, and ephemeral gully erosion evolution by using rare earth elements as tracers. *J. Hydrol.* **2022**, *612*, 128271. [CrossRef]
14. Casalí, J.; Loizu, J.; Campo, M.; De Santisteban, L.; Álvarez-Mozos, J. Accuracy of methods for field assessment of rill and ephemeral gully erosion. *Catena* **2006**, *67*, 128–138. [CrossRef]
15. Wang, R.; Sun, H.; Yang, J.; Zhang, S.; Fu, H.; Wang, N.; Liu, Q. Quantitative evaluation of gully erosion using multitemporal UAV data in the southern black soil region of Northeast China: A case study. *Remote Sens.* **2022**, *14*, 1479. [CrossRef]
16. Ghosh, S.; Kundu, S. Morphometric characterization and erosion assessment of gullies in the lateritic badlands of Eastern India using ALOS AW3D30 DEM and topographic indices. *Geocarto Int.* **2022**, *37*, 10096–10129. [CrossRef]
17. Fei, J.; Liu, J.; Ke, L.; Wang, W.; Wu, P.; Zhou, Y. A deep learning-based method for mapping alpine intermittent rivers and ephemeral streams of the Tibetan Plateau from Sentinel-1 time series and DEMs. *Remote Sens. Environ.* **2022**, *282*, 113271. [CrossRef]
18. Gafurov, A. Mapping of rill erosion of the middle volga (Russia) region using deep neural network. *ISPRS Int. J. Geo-Inf.* **2022**, *11*, 197. [CrossRef]
19. Liu, B.; Zhang, B.; Yin, Z.; Hao, B.; Wu, S.; Feng, H.; Siddique, K.H. Ephemeral gully development in the hilly and gully region of China's loess plateau. *Land Degrad. Dev.* **2024**, *35*, 128–141. [CrossRef]
20. Kılıç, M.; Gündoğan, R.; Günal, H.; Budak, M. An integrated framework to identify and map gullies in a Mediterranean region of Turkey. *Geocarto Int.* **2022**, *37*, 12846–12866. [CrossRef]
21. Hasanuzzaman, M.; Shit, P.K.; Alqadhi, S.; Almohamad, H.; Hasher, F.F.b.; Abdo, H.G.; Mallick, J. Utilizing machine learning algorithms for the development of Gully Erosion susceptibility maps: Evidence from the Chotanagpur Plateau Region, India. *Sustainability* **2024**, *16*, 6569. [CrossRef]
22. Liu, B.; Zhang, B.; Feng, H.; Wu, S.; Yang, J.; Zou, Y.; Siddique, K.H. Ephemeral gully recognition and accuracy evaluation using deep learning in the hilly and gully region of the Loess Plateau in China. *Int. Soil Water Conserv. Res.* **2022**, *10*, 371–381. [CrossRef]
23. Mohebzadeh, H.; Biswas, A.; DeVries, B.; Rudra, R.; Daggupati, P. Transferability of predictive models to map susceptibility of ephemeral gullies at large scale. *Nat. Hazards* **2024**, *120*, 4527–4561. [CrossRef]
24. Wang, Z.; Zhang, G.; Wang, C.; Xing, S. Assessment of the gully erosion susceptibility using three hybrid models in one small watershed on the Loess Plateau. *Soil Tillage Res.* **2022**, *223*, 105481. [CrossRef]
25. Fathololoumi, S.; Vasava, H.B.; Saurette, D.; Daggupati, P.; Biswas, A. Enhanced ephemeral gully mapping through multi-classifier integration and spectral feature analysis. *Catena* **2025**, *248*, 108590. [CrossRef]
26. Perras, M.A.; Diederichs, M.S.; Besaw, D. Geological and geotechnical observations from the Niagara Tunnel Project. *Bull. Eng. Geol. Environ.* **2014**, *73*, 1303–1323. [CrossRef]
27. Banks, W.D.; Brunton, F.R. Collaboration between Ontario Geological Survey, consultants and municipal staff results in discovery and development of a safe and sustainable bedrock groundwater supply for the town of Shelburne, southern Ontario, Canada. In Proceedings of the GeoOttawa 2017 IAH-CNC 70th Canadian Geotechnical Conference & 12th Joint CGS/IAH-CNC Groundwater Conference, Ottawa, ON, Canada, 1–4 October 2017.
28. Bannari, A.; Morin, D.; Bonn, F.; Huete, A. A review of vegetation indices. *Remote Sens. Rev.* **1995**, *13*, 95–120. [CrossRef]
29. Escadafal, R.; Belghit, A.; Ben-Moussa, A. Indices spectraux pour la télédétection de la dégradation des milieux naturels en Tunisie aride. In Proceedings of the 6th International Symposium on Physical Measurements and Signatures in Remote Sensing, Val d'Isere, France, 17–21 January 1994; pp. 17–21.
30. McFeeters, S.K. The use of the Normalized Difference Water Index (NDWI) in the delineation of open water features. *Int. J. Remote Sens.* **1996**, *17*, 1425–1432. [CrossRef]
31. Breiman, L. Random forests. *Mach. Learn.* **2001**, *45*, 5–32. [CrossRef]
32. Rigatti, S.J. Random forest. *J. Insur. Med.* **2017**, *47*, 31–39. [CrossRef]

33. Sheshukov, A.Y.; Sekaluvu, L.; Hutchinson, S.L. Accuracy of topographic index models at identifying ephemeral gully trajectories on agricultural fields. *Geomorphology* **2018**, *306*, 224–234. [CrossRef]
34. Yibeltal, M.; Tsunekawa, A.; Haregeweyn, N.; Adgo, E.; Meshesha, D.T.; Masunaga, T.; Tsubo, M.; Billi, P.; Ebabu, K.; Fenta, A.A. Morphological characteristics and topographic thresholds of gullies in different agro-ecological environments. *Geomorphology* **2019**, *341*, 15–27. [CrossRef]
35. Karydas, C.; Panagos, P. Towards an assessment of the ephemeral gully erosion potential in Greece using Google Earth. *Water* **2020**, *12*, 603. [CrossRef]
36. Castillo, C.; Taguas, E.V.; Zarco-Tejada, P.; James, M.R.; Gómez, J.A. The normalized topographic method: An automated procedure for gully mapping using GIS. *Earth Surf. Process. Landf.* **2014**, *39*, 2002–2015. [CrossRef]
37. Shahabi, H.; Jarihani, B.; Tavakkoli Piralilou, S.; Chittleborough, D.; Avand, M.; Ghorbanzadeh, O. A semi-automated object-based gully networks detection using different machine learning models: A case study of Bowen catchment, Queensland, Australia. *Sensors* **2019**, *19*, 4893. [CrossRef]
38. Shruthi, R.B.; Kerle, N.; Jetten, V. Object-based gully feature extraction using high spatial resolution imagery. *Geomorphology* **2011**, *134*, 260–268. [CrossRef]
39. Shruthi, R.B.; Kerle, N.; Jetten, V.; Abdellah, L.; Machmach, I. Quantifying temporal changes in gully erosion areas with object oriented analysis. *Catena* **2015**, *128*, 262–277. [CrossRef]
40. Desprats, J.-F.; Raclot, D.; Rousseau, M.; Cerdan, O.; Garcin, M.; Le Bissonnais, Y.; Ben Slimane, A.; Fouché, J.; Monfort-Climent, D. Mapping linear erosion features using high and very high resolution satellite imagery. *Land Degrad. Dev.* **2013**, *24*, 22–32. [CrossRef]
41. Pimentel, D. Soil erosion: A food and environmental threat. *Environ. Dev. Sustain.* **2006**, *8*, 119–137. [CrossRef]
42. Lal, R. Soil degradation by erosion. *Land Degrad. Dev.* **2001**, *12*, 519–539. [CrossRef]
43. Montgomery, D.R. Soil erosion and agricultural sustainability. *Proc. Natl. Acad. Sci. USA* **2007**, *104*, 13268–13272. [CrossRef]
44. Lal, R. Soil erosion and the global carbon budget. *Environ. Int.* **2003**, *29*, 437–450. [CrossRef]
45. Foley, J.A.; DeFries, R.; Asner, G.P.; Barford, C.; Bonan, G.; Carpenter, S.R.; Chapin, F.S.; Coe, M.T.; Daily, G.C.; Gibbs, H.K. Global consequences of land use. *Science* **2005**, *309*, 570–574. [CrossRef]
46. Turner, B.L.; Lambin, E.F.; Reenberg, A. The emergence of land change science for global environmental change and sustainability. *Proc. Natl. Acad. Sci. USA* **2007**, *104*, 20666–20671. [CrossRef] [PubMed]
47. Foley, J.A.; Ramankutty, N.; Brauman, K.A.; Cassidy, E.S.; Gerber, J.S.; Johnston, M.; Mueller, N.D.; O'Connell, C.; Ray, D.K.; West, P.C. Solutions for a cultivated planet. *Nature* **2011**, *478*, 337–342. [CrossRef] [PubMed]
48. Tilman, D.; Cassman, K.G.; Matson, P.A.; Naylor, R.; Polasky, S. Agricultural sustainability and intensive production practices. *Nature* **2002**, *418*, 671–677. [CrossRef] [PubMed]
49. Godfray, H.C.J.; Beddington, J.R.; Crute, I.R.; Haddad, L.; Lawrence, D.; Muir, J.F.; Pretty, J.; Robinson, S.; Thomas, S.M.; Toulmin, C. Food security: The challenge of feeding 9 billion people. *Science* **2010**, *327*, 812–818. [CrossRef]

Disclaimer/Publisher's Note: The statements, opinions and data contained in all publications are solely those of the individual author(s) and contributor(s) and not of MDPI and/or the editor(s). MDPI and/or the editor(s) disclaim responsibility for any injury to people or property resulting from any ideas, methods, instructions or products referred to in the content.